Radiolabeled RGD Uptake and α_v Integrin Expression Is Enhanced in Ischemic Murine Hindlimbs

Kyung-Han Lee, MD[1]; Kyoung-Ho Jung, BA[1]; Sung-Hee Song, MS[1]; Dong Hyun Kim, BA[1]; Byung Chul Lee, PhD[2]; Hyun Ju Sung, MS[2]; Yu-Mi Han, MS[3]; Yearn Seong Choe, PhD[1]; Dae Yoon Chi, PhD[2]; and Byung-Tae Kim, MD[1]

[1]Department of Nuclear Medicine, Samsung Medical Center, Sungkyunkwan University School of Medicine, Seoul, Korea; [2]Department of Chemistry, College of Medicine, Inha University, Inchun, Korea; and [3]Department of Anatomy, College of Medicine, Inha University, Inchun, Korea

Radiolabeled RGD peptides that target $\alpha_v\beta_3$ integrin are promising tracers for imaging tumor angiogenesis. Integrins and angiogenesis also play important roles in healing of ischemic lesions. Thus, we investigated the biodistribution of radiolabeled RGD and expression of α_v integrin in a mouse model of hindlimb ischemia. **Methods:** ^{125}I-3-Iodo-D-Tyr^4-cyclo(-Arg-Gly-Asp-D-Tyr-Val-) (^{125}I-c(RGD(I)yV)) was synthesized and tested for endothelial binding. Hindlimb ischemia was induced in ICR mice through femoral artery ablation, and perfusion was measured with laser Doppler blood flowmetry. ^{125}I-c(RGD(I)yV) biodistribution was evaluated in control animals ($n = 7$) and ischemic models on day 3, 8, or 14 ($n = 6$ each). Control experiments were performed using a radiolabeled peptide with a scrambled amino acid sequence (^{125}I-GfVGV). Microsections of hindlimb tissue were immunostained for α_v integrin expression and stained with alkaline phosphatase to localize vascular endothelial cells. **Results:** ^{125}I-c(RGD(I)yV) retained specific binding to human umbilical vein endothelial cells. Perfusion in ischemic hindlimbs immediately fell to 10% ± 4% of contralateral levels and gradually recovered to 22% ± 11% and 64% ± 9% on days 8 and 14, respectively. ^{125}I-c(RGD(I)yV) uptake in ischemic muscles significantly increased from a control level of 0.16 ± 0.05 %ID/g (percentage injected dose per gram of tissue) to 0.85 ± 0.76 %ID/g at day 3, 0.43 ± 0.23 %ID/g at day 8, and 0.43 ± 0.28 %ID/g at day 14 (all $P < 0.05$). Ischemic muscle-to-lung count ratios had a virtually identical trend: 0.42 ± 0.25 for controls, 2.34 ± 1.70 at day 3 ($P < 0.02$), 1.46 ± 0.52 at day 8 ($P < 0.001$), and 1.39 ± 0.94 at day 14 ($P < 0.02$). In contrast, uptake of the control peptide in ischemic hindlimbs was not different from that of controls. Immunohistochemistry revealed substantially increased α_v integrin staining in ischemic hindlimb tissue. **Conclusion:** Radioiodine RGD uptake is significantly enhanced in ischemic hindlimbs of a mouse model, and is accompanied by an increase in α_v integrin expression. Further investigation is thus warranted to illuminate the potential role of radiolabeled RGD for noninvasive monitoring of peripheral ischemic lesions.

Key Words: RGD peptides; integrin; ischemia; angiogenesis;
J Nucl Med 2005; 46:472–478

Recent developments in therapeutic strategies to modulate new vessel formation, a crucial component of various disease processes (*1*), have provided a myriad of molecular targets that may be exploited for angiogenesis imaging. One of the most promising of imaging probes are RGD peptides that target and bind specifically to $\alpha_v\beta_3$ integrin (*2*), a cell-surface receptor highly restricted in expression to angiogenic vasculature (*3*). Hence, several radiolabeled RGD probes have been developed for $\alpha_v\beta_3$ integrin imaging and have been extensively investigated in tumor animal models (*4–8*).

However, angiogenesis is not only involved in cancer progression but also plays an important part in the improvement and healing of ischemic lesions (*9,10*). Accordingly, elevated $\alpha_v\beta_3$ integrin expression has been observed in ischemic tissue of the brain (*11*), retina (*12*), and muscles (*13–15*). Recently, increased $\alpha_v\beta_3$ integrin expression in injured vasculature and infarcted myocardium has been successfully imaged with ^{111}In-labeled quinolone (*16,17*). In addition, microbubbles labeled with echistatin or anti-α_v antibody have been shown to allow noninvasive imaging of α_v integrin expression in angiogenic vessels of matrigel plug and tumor models (*18,19*). In this study, we hypothesized that radiolabeled RGD uptake may be elevated in peripheral ischemic lesions in association with an increase in local α_v integrin expression. To test this hypothesis, we investigated the biodistribution of radioiodine-labeled cyclic RGD and immunostaining of α_v integrin in a mouse model of hindlimb ischemia.

MATERIALS AND METHODS

Biologic Assays

For endothelial cell binding experiments, ^{125}I-3-iodo-D-Tyr^4-cyclo(-Arg-Gly-Asp-D-Tyr-Val-) (^{125}I-c(RGD(I)yV)) was pre-

Received Mar. 6, 2004; revision accepted Oct. 21, 2004.
For correspondence or reprints contact: Kyung-Han Lee, MD, Department of Nuclear Medicine, Samsung Medical Center, 50 Ilwondong, Kangnamgu, Seoul, Korea.
E-mail: khnm.lee@samsung.com

pared and purified by high-performance liquid chromatography essentially following previously described procedures (*4*). Human umbilical vein endothelial cells (HUVEC-C; American Type Culture Collection) were cultured at 37°C and 5% CO_2 in EBM-2 media containing endothelial growth supplements, 10% fetal bovine serum, and antibiotics. Cells of 80%–90% confluence were harvested with trypsin, washed twice with Dulbecco's phosphate-buffered saline (D-PBS), and 10^5 to 10^6 cells were transferred to Eppendorf tubes. After incubation with 37 kBq ^{125}I-c(RGD(I)yV) at 37°C for indicated durations, cells were rapidly washed twice with D-PBS and measured for bound radioactivity on a γ-counter. For competitive binding experiments, cell binding after 1-h incubation was measured, but with 0, 1, 10, or 100 μmol/L of nonradiolabeled c(RGD(I)yV). A displacement curve was plotted and the 50% inhibitory concentration was calculated using GraphPad Prism version 3.02 software (GraphPad Software Inc.). All experiments were performed in duplicates, and results are expressed as mean ± SD of the percentage of cell-bound counts relative to the 15-min value or counts relative to the sample without addition of nonradiolabeled c(RGD(I)yV).

Animal Model

Unilateral hindlimb ischemia was created in 8- to 10-wk-old male ICR mice following animal protocols approved by the Institutional Regulatory Board. Animals were anesthetized by intraperitoneal administration of xylazine and ketamine for ischemia surgery, laser Doppler flowmetry, and scintigraphic imaging. To induce hindlimb ischemia, a vertical incision was applied on the skin overlying the left femoral region, femoral vessels were exposed, and the femoral artery was carefully separated and excised after ligation of the proximal and distal ends.

A laser Doppler blood flow meter (Moor Instruments) was used to evaluate perfusion in hindlimbs immediately after ischemia surgery and again just before biodistribution studies. Mice were anesthetized, shaved, depilated on the ventral side of hindlimbs with depilatory cream, and placed on a 37°C heating plate to minimize temperature variation. Perfusion signals were displayed and recorded in color codes ranging from dark blue (0) to red to white (1,000). Regions of interests (ROIs) were drawn along the outlines of hindlimbs from which average signal levels were measured, and the perfusion level of an ischemic limb was expressed as its mean signal ratio relative to that of the contralateral side.

Biodistribution Studies and Scintigraphic Imaging

Biodistribution studies were performed by tail vein injection of mice with 370 kBq of ^{125}I-c(RGD(I)yV). To correct for any radiotracer retained within the delivery system, a syringe containing radiotracer was emptied into an Eppendorf tube and 1/10 and 1/100 aliquots were transferred and counted as 10% and 1% injected dose (ID) standards. Piloting was first performed after 3 d of ischemia to compare 1- and 4-h distribution (n = 3 each), and 4 h was selected as the distribution time for the remaining experiments, which were performed after 3, 8, or 14 d of ischemia (n = 6, each). Immediately after animals were sacrificed by cervical dislocation, major organs, blood, and bilateral hindlimb thigh muscles were extracted, weighed, and measured for radioactivity on a γ-counter. Tails were also counted to correct for any radiotracer leakage during injection. Results are expressed as the percentage injected dose per gram (%ID/g) of tissue for each organ and as ischemic muscle-to-organ count ratios. Animals that did not undergo ischemia surgery were used as controls (n = 7).

To test specificity of radiotracer uptake, a peptide with the scrambled amino acid sequence GfVGV was ^{125}I labeled by the IODO-GEN method and used as a control peptide: ^{1}H NMR (400 MHz, D_2O) δ 7.18 (d, J = 8.4 Hz, 2H), 6.85 (d, J = 8.4 Hz, 2H), 4.72–4.66 (m, 1H), 4.10–4.01 (m, 2H), 4.00 (d, J = 5.6 Hz, 1H), 3.97–3.92 (m, 2H), 3.27 (dd, J = 16, 5.2 Hz, 1H)), 2.84 (dd, J = 14.4, 10.8 Hz, 1H), 2.27–2.19 (m, 1H), 1.84–1.75 (m, 1H), 1.05 (d, J = 6.8 Hz, 6H), 0.68 (d, J = 6.8 Hz, 3H), 0.64 (d, J = 6.8 Hz, 3H); calcd for $C_{23}H_{35}N_5O_7$ MALDI-TOF MS ($M + H^+$) = 494.41. Control mice (n = 4) and animals at 8 d of hindlimb ischemia (n = 5) were injected with the control radiopeptide and evaluated for biodistribution.

Scintigraphic imaging was performed in 2 mice on day 3 of hindlimb ischemia. A single 30-min scintigraphic image was acquired on a γ-camera (Monad XLT; Trionix Research Laboratory) equipped with a pinhole collimator at 4 h after intravenous injection of 2.6 MBq ^{123}I-c(RGD(I)yV). For quantitative analysis, image window scales were first adjusted to enhance contrast between hindlimb and background, and a polygonal ROI was manually drawn along the margin of the thigh, from the knee region up to the proximal thigh but sufficiently below abdominal radioactivity. ROIs were drawn first on the ischemic thigh and another of similar shape and size was then applied to the contralateral side. ROI selection with count ratio determination was repeated twice and showed good reproducibility.

Immunohistochemistry and Histology

After measurement of ^{125}I-c(RGD(I)yV) uptake levels, the dissected hindlimb muscles were fixed with Bouin's solution. Cryostat sections of 10-μm thickness were mounted on glass slides and immunostained using the avidin–biotin–peroxidase technique. Sections were incubated at 4°C for 16 h with a rabbit polyclonal antibody against the mouse α_v integrin subunit (Chemicon International) at 1:1,000 dilution in TBS (100 mmol/L Tris, pH 7.4, 138 mmol/L NaCl, 27 mmol/L KCl) containing 1% bovine serum albumin. The sections were then incubated with a biotinylated antirabbit secondary antibody at room temperature for 1 h. After the avidin/biotinylated enzyme complex was applied (Vector Laboratories), the immunoreaction was cytochemically revealed by H_2O_2 diaminobenzidine hydrochloride solution (Sigma).

Alkaline phosphatase staining was used as a specific marker of vascular endothelial cells in microsections immediately contiguous to those used for immunostaining. Hematoxylin and eosin staining was performed for morphologic evaluation and to identify regions of focal inflammatory cell infiltration.

RESULTS

Specific Endothelial Cell Binding of ^{125}I-c(RGD(I)yV)

HUVEC-C cell binding studies showed a gradual increase in ^{125}I-c(RGD(I)yV) uptake over 4 h (Fig. 1A), and subsequent cell experiments were performed with 1-h incubation. The presence of unlabeled c(RGD(I)yV) resulted in a concentration-dependent inhibition of endothelial ^{125}I-c(RGD(I)yV) binding, with a calculated 50% inhibitory concentration (IC_{50}) of 227 nmol/L (Fig. 1B).

Blood Flow and ^{125}I-c(RGD(I)yV) Uptake in Hindlimb Ischemia Models

There was a precipitous reduction of hindlimb perfusion immediately after femoral artery removal, resulting in flow

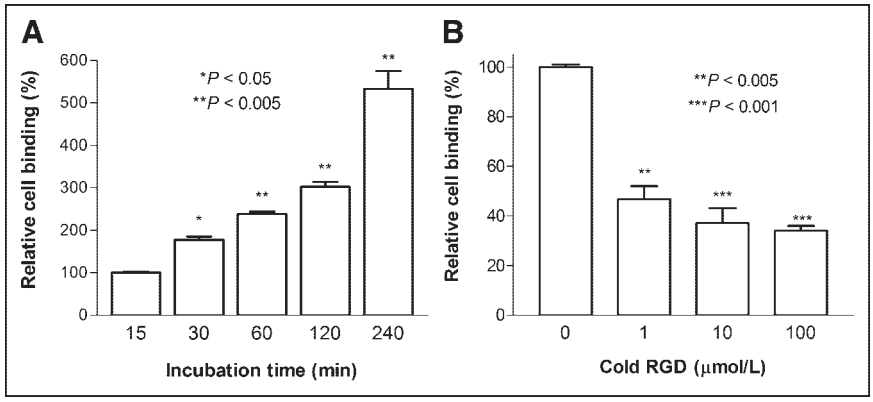

FIGURE 1. Endothelial cell binding of ^{125}I-c(RGD(I)yV). (A) Incubation time-dependent increase of ^{125}I-c(RGD(I)yV) binding to HUVEC cells. Results are expressed as percent uptake relative to 15-min value. (B) Dose-dependent inhibition of cell binding by excess nonradiolabeled c(RGD(I)yV). Results are expressed as percent uptake relative to sample without nonradiolabeled c(RGD(I)yV). All results are mean ± SD of duplicates.

ratios of 0.10 ± 0.04. Flow ratios remained at 0.09 ± 0.03 on day 3 but gradually recovered thereafter to 0.22 ± 0.11 at day 8 and 0.64 ± 0.09 at day 14 ($P < 0.05$ and <0.0001 compared with immediate postoperative ratios, respectively; Figs. 2A and 2B).

Piloting of 1- and 4-h ^{125}I-c(RGD(I)yV) distribution showed slightly higher ischemic muscle-to-blood ratios at 4 h (data not shown), which was selected for the remaining experiments. In normal ICR mice, 4-h biodistribution of ^{125}I-c(RGD(I)yV) (Table 1) was similar to that previously reported for BALB/c and nude mice (*4*). The highest uptakes were seen in the liver and kidneys (0.68 ± 0.37 %ID/g and 0.85 ± 0.27 %ID/g, respectively), whereas normal hindlimb muscle had relatively low uptake (0.16 ± 0.05 %ID/g). In the ischemic model, uptake in the ischemic muscles was significantly increased to 0.85 ± 0.76 %ID/g on day 3, 0.43 ± 0.23 %ID/g on day 8, and 0.43 ± 0.28 %ID/g on day 14 (all $P < 0.05$) (Table 1; Fig. 3A). However, there was considerable individual variability of ischemic muscle uptake on day 3. Ischemic limb muscle-to-lung uptake ratios revealed a temporal pattern virtually identical to that of %ID/g uptake levels (Fig. 3B). In contrast, uptake of the control peptide in ischemic hindlimbs at 8 d was not different from that of control animal hindlimbs (0.11 ± 0.05 %ID/g vs. 0.12 ± 0.05 %ID/g; P = not significant [NS]; Fig. 4A) and in muscle-to-lung uptake ratios (0.51 ± 0.21 vs. 0.38 ± 0.18; P = NS; Fig. 4B).

Scintigraphic ^{123}I-c(RGD(I)yV) Imaging in Hindlimb Ischemia Models

Scintigraphic ^{123}I-c(RGD(I)yV) images of mice at day 3 of ischemia showed better visualization of the ischemic hindlimbs compared with the contralateral hindlimbs (Fig. 5). Although activity in the liver, kidneys, and intestines was high, these activities did not interfere with assessment of limb activity. ROI analysis revealed an ischemic-to-contralateral limb count ratio of 1.8 ± 0.4.

Histologic Findings

The histology sections were of somewhat less than optimum quality due to the severe architectural disruption caused by the ischemic injury. Hematoxylin and eosin staining of ischemic hindlimb muscles demonstrated muscle injury with irregular regions of necrosis and inflammatory cell infiltration (Figs. 6A, 6C, 6E, and 6G). Immunostaining revealed pronounced positive staining for α_v integrin in ischemic but not in control hindlimb tissue (Figs. 6B, 6D, 6F, and 6H). Alkaline phosphatase staining confirmed part of the α_v staining to localize to vascular endothelial cells (Figs. 7A and 7B) and a large portion of α_v staining appeared to localize to skeletal myocytes (Fig. 7C). In con-

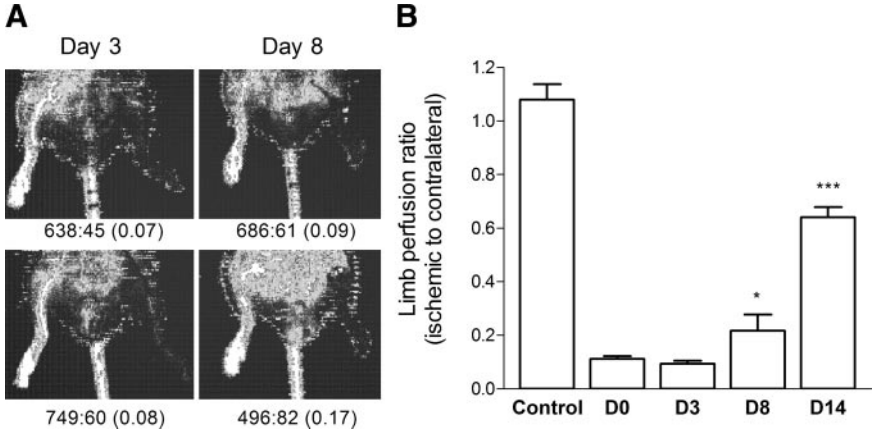

FIGURE 2. Hindimb blood flow monitored with laser Doppler flowmetry. (A) Doppler images of representative animals on days 3 and 8 of ischemia. Right:left hindlimb flow measurements (perfusion ratios in parentheses) are denoted below each image. (B) Temporal change of right-to-left hindlimb perfusion ratios. There was severe hypoperfusion in left hindlimb immediately after surgery (D0) and on day 3 (D3), which gradually improved on day 8 (D8) and day 14 (D14). Data are shown as mean ± SD of left-to-right ratios. *$P < 0.05$; ***$P < 0.0001$ compared with immediate postoperative ratios.

TABLE 1
Biodistribution of ^{125}I-c(RGD(I)yV) in Control and Hindlimb Ischemic Mice

Tissue	Control (n = 8)	Hindlimb ischemia model		
		3 d (n = 6)	8 d (n = 6)	14 d (n = 6)
Blood	0.41 ± 0.20	0.39 ± 0.09	0.28 ± 0.07	0.31 ± 0.10
Heart	0.18 ± 0.09	0.20 ± 0.04	0.12 ± 0.03	0.13 ± 0.04
Lung	0.43 ± 0.19	0.38 ± 0.15	0.29 ± 0.08	0.30 ± 0.09
Liver	0.68 ± 0.37	0.99 ± 0.24	1.05 ± 0.33	0.60 ± 0.23
Spleen	0.29 ± 0.12	0.32 ± 0.07	0.23 ± 0.04	0.23 ± 0.12
Pancreas	0.16 ± 0.09	0.24 ± 0.06	0.14 ± 0.06	0.15 ± 0.04
Kidneys	0.85 ± 0.27	1.02 ± 0.31	0.84 ± 0.19	0.63 ± 0.27
Hindlimb muscle*	0.16 ± 0.05	0.85 ± 0.76†	0.43 ± 0.23†	0.43 ± 0.28†

*Ischemic limb for ischemic models and average of both limbs for controls.
†$P < 0.05$ compared with control values.
Values are expressed as mean ± SD of %ID/g of tissue at 4 h after injection.

trast, sites of inflammatory cell infiltration did not show significant α_v staining (Fig. 7D).

DISCUSSION

Whereas the biokinetics of radiolabeled RGD has been extensively investigated in tumor-bearing animals (*4–8*), our study concentrated on mice with hindlimb ischemia, which is a commonly used animal model of human occlusive peripheral vascular disease (*20*). Peripheral ischemic disease is a leading cause of jeopardized limb viability, and therapeutic angiogenesis has recently emerged as a promising strategy for its treatment (*21,22*). Accordingly, the development of noninvasive imaging methods to monitor the healing process of peripheral ischemic lesions would be of significant clinical benefit.

In this study, ^{125}I-c(RGD(I)yV) was first tested for specificity of endothelial cell binding. Although the binding experiments were less than optimal because nanomolar ranges of nonradiolabeled RGD were not included and remnant binding in the presence of maximal RGD doses suggests insufficient blocking of nonspecific binding, the results confirmed that the radiotracer retains specific endothelial binding characteristics.

The results of our biodistribution experiments demonstrate a significantly enhanced uptake of radioiodine-labeled RGD in mouse hindlimb tissue exposed to ischemia. There was a >5-fold increase in the level of ischemic hindlimb radiouptake expressed in %ID/g and muscle-to-lung count ratios. Both indices of uptake demonstrated a very similar temporal pattern, showing a peak at day 3 and maintaining a slightly lower, but increased, level at 8 and 14 d of ischemia. The lack of increase in control peptide uptake supports specific uptake of ^{125}I-c(RGD(I)yV) in ischemic hindlimbs rather than nonspecific leakage through injured vasculature. Ischemic-to-contralateral limb ratios of radiotracer uptake were also increased (1.60 ± 0.72, 2.69 ± 1.17, 3.43 ± 1.85 at days 3, 8, and 14, respectively), but the ratio at day 3 was not as high as the %ID/g or ischemic muscle-to-lung ratios due to an unexplainable uptake increase in the contralateral hindlimbs as well as ischemic hindlimbs in a few animals. This may be related to greater weight bearing or some remote effect to the contralateral limb.

The ischemia group also appeared to have higher hepatic and renal uptake (although not to a statistically significant degree), with a temporal pattern similar to that of the ischemic hindlimbs. Though the precise cause for this find-

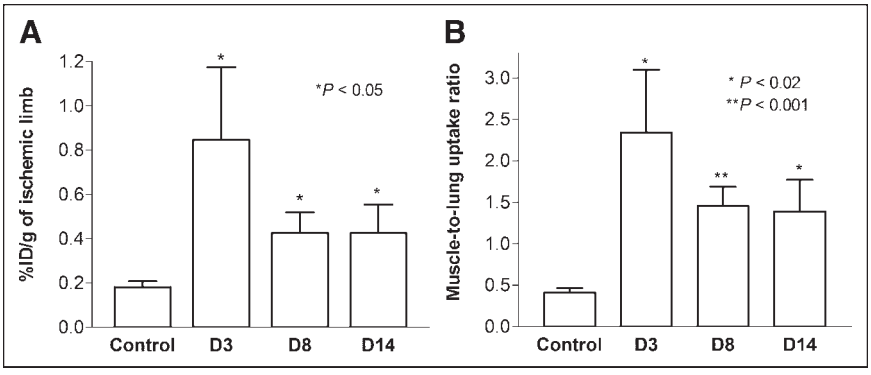

FIGURE 3. ^{125}I-c(RGD(I)yV) uptake in ischemic hindlimbs according to periods of ischemia. ^{125}I-c(RGD(I)yV) uptake in ischemic hindlimb muscles is expressed as %ID/g (A) and muscle-to-lung uptake ratios (B). Data are expressed as mean ± SD of 6 animals for each ischemia period and 7 animals for control.

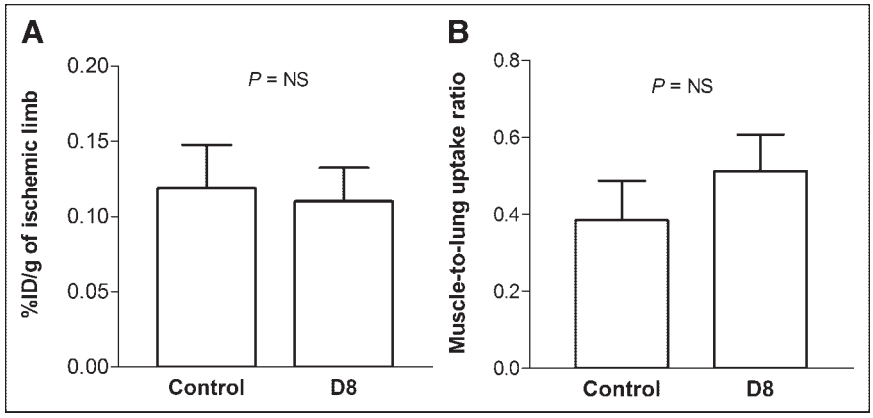

FIGURE 4. Uptake of control peptide (^{125}I-GfVGV). Uptake in muscle tissue of ischemic hindlimb and hindlimb of control animals is expressed as %ID/g (A) and muscle-to-lung uptake ratios (B). Data are shown as mean ± SD of 5 ischemic hindlimb models and 4 control animals.

ing is not clear, it should be noted that hindlimb ischemia is known to cause multiple organ dysfunction with evidence of hepatic and renal damage (*23,24*). However, determination of whether such tissue damage was present in our animal model and whether it was associated with an increase in integrin expression will require further investigation.

Scintigraphic images were evaluated by comparing ischemic hindlimb uptake to the contralateral side because control animals were not imaged, and the results showed relatively higher uptake in the ischemic side. Although uptake in angiogenic surgical wounds may overlap with muscle activity on planar images, the narrow linear surgical wound in the midline region is not likely to have significantly affected the diffuse uptake we observed throughout the entire thigh area. The modest image contrast between ischemic and contralateral hindlimb in our study is partly contributed from the low tracer dose (2.6 MBq) that was used to image the small muscle mass of mice and may be improved with larger tracer doses. The images verified high liver and intestinal radiouptake, which is attributed to the tracer's hydrophobic nature (*4*) and significantly limits its usefulness for evaluating lesions within or near the abdomen. Therefore, further experiments with regard to imaging of ischemic lesions would benefit from using one of the more recently introduced RGD compounds that have improved imaging properties, such as less hepatic clearance and longer circulation time, which allows higher uptake in skeletal muscle (*6*).

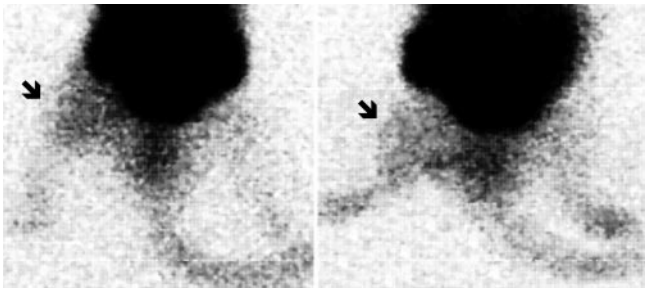

FIGURE 5. Scintigraphic ^{123}I-c(RGD(I)yV) images in hindlimb ischemic models on day 3 demonstrate higher radioactivity in ischemic left (arrows) compared with contralateral hindlimbs.

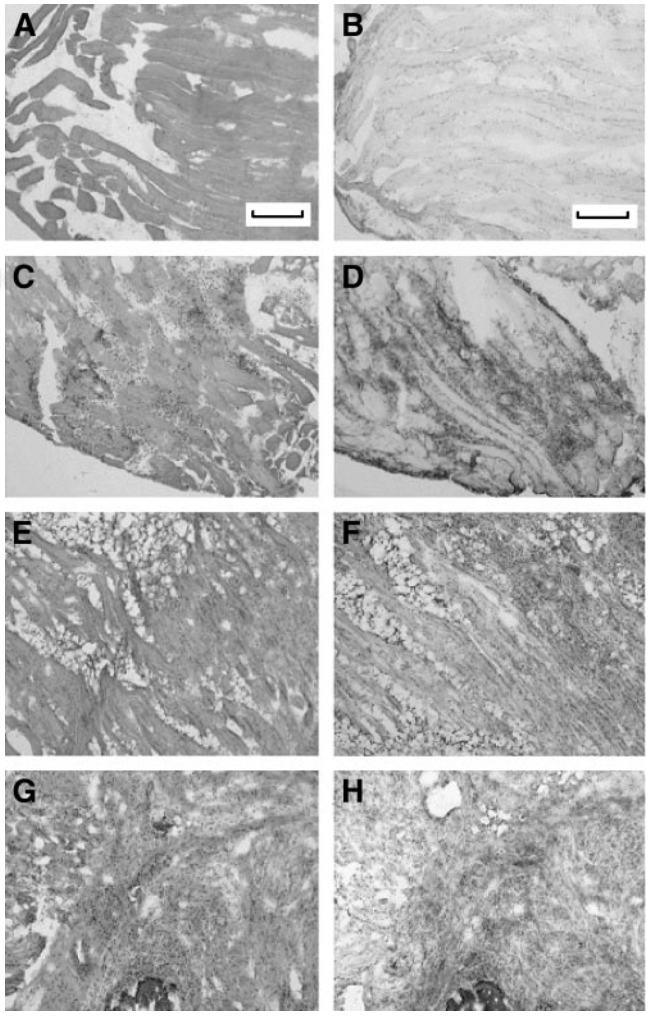

FIGURE 6. Immunohistochemical detection of α_v integrin. Hematoxylin and eosin staining (A, C, E, G) and α_v integrin immunostaining (B, D, F, H) of hindlimb muscle tissue microsections. Tissues are from normal control animals (A and B) and mice at 3 d (C and D), 8 d (E and F), and 14 d (G and H) of ischemia. Length of bar indicates 400 μm.

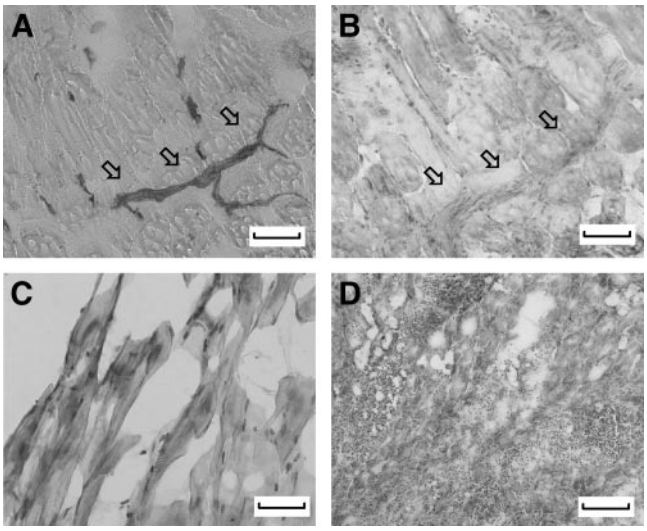

FIGURE 7. Histologic localization of α_v integrin staining. Alkaline phosphatase staining (A) demonstrates localization of α_v integrin immunoreactivity (B) to vascular endothelial cells. High magnification shows α_v integrin immunostaining localized to skeletal muscle cells (C). Hematoxylin and eosin counterstaining shows lack of α_v immunostaining in inflammatory cell infiltration sites (D). Length of bar indicates 200 μm for A, B, and D and 100 μm for C.

Immunohistochemical staining revealed that the elevated radioprobe uptake was accompanied by an increase in α_v integrin expression levels. This finding is of significant interest because α_v integrin has important roles in angiogenesis and ischemia (*25*). Though it is possible that α_v integrin heterodimers other than $\alpha_v\beta_3$, such as $\alpha_v\beta_5$, also contributed—since ^{125}I-c(RGD(I)yV) has substantially higher selectivity for $\alpha_v\beta_3$ integrin compared with $\alpha_{IIb}\beta_3$ or $\alpha_v\beta_5$ (*4,6*)—$\alpha_v\beta_3$ appears to be the most likely candidate responsible for the observed α_v staining. Nevertheless, staining of β_3 integrin in addition to $\alpha_v\beta_3$ staining would have provided more supporting evidence for $\alpha_v\beta_3$ binding of the radiotracer.

The concomitant increase in integrin immunoreactivity suggests that radiolabeled RGD uptake may be enhanced in ischemic limbs as a result of an increase in local integrin binding. RGD sequences form an essential recognition site for integrin (*26,27*), which are cell-surface receptors that mediate cell–cell as well as cell–matrix interactions. $\alpha_v\beta_3$ integrins are an important player in angiogenesis and are also involved in cytoskeleton rearrangement, wound healing, cell proliferation, and repair responses to tissue damage (*28–30*). Modifications in integrin expression appear necessary in ischemic tissue not only for improved perfusion through angiogenesis but also for remodeling processes to generate new connections between viable cells and new matrix. In specimen of inflamed human muscle tissue with hypoxic and ischemic injury, Konttinen et al. observed increased β_3 integrin immunoreactivity in blood vessels, myocyte sarcolemma, and basal laminae (*15*). In a rat model of myocardial ischemia, Sun et al. found that myocardial β_1 and β_3 integrin expression was increased in a temporal pattern similar to the period that α_v integrin expression and RGD uptake was enhanced in our hindlimb ischemia model (*13*).

In addition to vascular structures, a large portion of α_v staining appeared to localize to skeletal myocytes within the ischemic tissue. $\alpha_v\beta_3$ integrins are expressed not only on activated endothelial cells but also on fibroblasts, smooth muscle, and some types of tumor cells. Skeletal myocytes also express a repertoire of integrins, including $\alpha_v\beta_3$ integrin (*15,31,32*). As cellular–extracellular matrix interactions provide a substrate essential for normal homeostasis and adaptation to pathophysiologic signals, it may be that integrin expression in skeletal muscle is modulated during the healing or remodeling processes of ischemic injury. Despite our immunostaining results, however, localization of α_v expression does not prove which types of cells actually take up the radiotracer, and clarification of this issue must be addressed in future investigations.

CONCLUSION

Radioiodine-labeled cRGD uptake is significantly enhanced in ischemic limb muscles. Further investigation is thus warranted to elucidate the potential role of radiolabeled RGD imaging for monitoring peripheral ischemic lesions.

ACKNOWLEDGMENTS

The authors are grateful for Dr. In-Sun Park for his helpful advice and thank Jin-Young Paik, Hye-Kyung Kim, and Bong-Ho Kho for technical assistance. This work was supported by the National Mid- and Long-term Nuclear R&D Program grant M20243010001-04A0701-00110 of the Korean Ministry of Science and Technology.

REFERENCES

1. Folkman J. Angiogenesis in cancer, vascular, rheumatoid and other disease. *Nat Med.* 1995;1:27–31.
2. Brooks PC, Clark RA, Cheresh DA. Requirement of vascular integrin $\alpha_v\beta_3$ for angiogenesis. *Science.* 1994;264:569–571.
3. Ruoslahti E, Pierschbacher MD. New perspectives in cell adhesion: RGD and integrins. *Science.* 1987;238:491–497.
4. Haubner R, Wester HJ, Reuning U, et al. Radiolabeled $\alpha_v\beta_3$ integrin antagonists: a new class of tracers for tumor targeting. *J Nucl Med.* 1999;40:1061–1071.
5. van Hagen PM, Breeman WA, Bernard HF, et al. Evaluation of a radiolabelled cyclic DTPA-RGD analogue for tumour imaging and radionuclide therapy. *Int J Cancer.* 2000;90:186–198.
6. Haubner R, Wester HJ, Burkhart F, et al. Glycosylated RGD-containing peptides: tracer for tumor targeting and angiogenesis imaging with improved biokinetics. *J Nucl Med.* 2001;42:326–336.
7. Haubner R, Wester HJ, Weber WA, et al. Noninvasive imaging of $\alpha_v\beta_3$ integrin expression using ^{18}F-labeled RGD-containing glycopeptide and positron emission tomography. *Cancer Res.* 2001;61:1781–1785.
8. Janssen ML, Oyen WJ, Dijkgraaf I, et al. Tumor targeting with radiolabeled $\alpha_v\beta_3$ integrin binding peptides in a nude mouse model. *Cancer Res.* 2002;62:6146–6151.
9. Baumgartner I, Pieczek A, Manor O, et al. Constitutive expression of VEGF 165 following intramuscular gene transfer promotes collateral vessel development in patients with critical limb ischemia. *Circulation.* 1998;97:1114–1123.
10. Banai S, Jaklitsch MT, Shou M, et al. Angiogenic-induced enhancement of

collateral blood flow to ischemic myocardium by vascular endothelial growth factor in dogs. *Circulation.* 1994;89:3964–3972.
11. Abumiya T, Lucero J, Heo JH, et al. Activated microvessels express vascular endothelial growth factor and integrin $\alpha_v\beta_3$ during focal cerebral ischemia. *J Cereb Blood Flow Metab.* 1999;19:1038–1050.
12. Takagi H, Suzuma K, Otani A, et al. Role of vitronectin receptor-type integrins and osteopontin in ischemia-induced retinal neovascularization. *Jpn J Ophthalmol.* 2002;46:270–278.
13. Sun M, Opavsky MA, Stewart DJ, et al. Temporal response and localization of integrins β_1 and β_3 in the heart after myocardial infarction: regulation by cytokines. *Circulation.* 2003;107:1046–1052.
14. Nawata J, Ohno I, Ishoyama S, et al. Differential expression of α_1, α_3 and α_5 integrin subunits in acute and chronic stages of myocardial infarction in rats. *Cardiovasc Res.* 1999;43:371–378.
15. Konttinen YT, Mackiewicz Z, Povilenaite D, Sukura A, Hukkanen M, Virtanen I. Disease-associated increased HIF-1, $\alpha_v\beta_3$ integrin, and Flt-1 do not suffice to compensate the damage-inducing loss of blood vessels in inflammatory myopathies. *Rheumatol Int.* 2004;24:333–339.
16. Sadeghi MM, Krassilnikova S, Zhang J, et al. Detection of injury-induced vascular remodeling by targeting activated $\alpha_v\beta_3$ integrin in vivo. *Circulation.* 2004;110:84–90.
17. Meoli DF, Sadeghi MM, Krassilnikova S, et al. Noninvasive imaging of myocardial angiogenesis following experimental myocardial infarction. *J Clin Invest.* 2004;113:1684–1691.
18. Leong-Poi H, Christiansen J, Klibanov AL, Kaul S, Lindner JR. Noninvasive assessment of angiogenesis by ultrasound and microbubbles targeted to α_v-integrins. *Circulation.* 2003;107:455–460.
19. Ellegala DB, Leong-Poi H, Carpenter JE, et al. Imaging tumor angiogenesis with contrast ultrasound and microbubbles targeted to $\alpha_v\beta_3$. *Circulation.* 2003;108:336–341.
20. Couffinhal T, Silver M, Zheng LP, Kearney M, Witzenbichler B, Isner JM. Mouse model of angiogenesis. *Am J Pathol.* 1998;152:1667–1679.
21. Rajagopalan S, Shah M, Luciano A, Crystal R, Nabel EG. Adenovirus-mediated gene transfer of VEGF(121) improves lower-extremity endothelial function and flow reserve. *Circulation.* 2001;104:753–755.
22. Shyu KG, Chang H, Wang BW, Kuan P. Intramuscular vascular endothelial growth factor gene therapy in patients with chronic critical leg ischemia. *Am J Med.* 2003;114:85–92.
23. Yassin MM, Harkin DW, Barros D'Sa AA, Halliday MI, Rowlands BJ. Lower limb ischemia-reperfusion injury triggers a systemic inflammatory response and multiple organ dysfunction. *World J Surg.* 2002;26:115–121.
24. Brock RW, Nie RG, Harris KA, Potter RF. Kupffer cell-initiated remote hepatic injury following bilateral hindlimb ischemia is complement dependent. *Am J Physiol Gastrointest Liver Physiol.* 2001;280:G279–G284.
25. Eliceiri BP, Cheresh DA. The role of α_v integrins during angiogenesis: insights into potential mechanisms of action and clinical development. *J Clin Invest.* 1999;103:1227–1230.
26. Plow EF, Haas TA, Zhang L, Loftus J, Smith JW. Ligand binding to integrins. *J Biol Chem.* 2000;275:21785–21788.
27. Pierschbacher MD, Ruoslahti E. The cell attachment activity of fibronectin can be duplicated by small fragments of the molecule. *Nature.* 1984;309:30–33.
28. Christofidou-Solomidou M, Bridges M, Murphy GF, Albelda SM, DeLisser HM. Expression and function of endothelial cell alpha v integrin receptors in wound induced human angiogenesis in human skin/SCID mice chimeras. *Am J Pathol.* 1997;151:975–983.
29. Sajid M, Stouffer GA. The role of $\alpha_v\beta_3$ integrins in vascular healing. *Thromb Haemost.* 2002;87:187–193.
30. Stouffer GA, Hu Z, Sajid M, et al. $\alpha_v\beta_3$ integrins are upregulated following vascular injury and mediate proliferation of cultured smooth muscle cells. *Circulation.* 1998;97:907–915.
31. Mayer U. Integrins: redundant or important players in skeletal muscle? *J Biol Chem.* 2003;278:14587–14590.
32. Balschuk KL, Guein C, Holland PC. Myoblast $\alpha_v\beta_3$ integrin levels are controlled by transcriptional regulation of expression of the β_3 subunit and down-regulation of the β_3 subunit is required for skeletal muscle cell differentiation. *Dev Biol.* 1997;184:266–277.

JNM The Journal of NUCLEAR MEDICINE

Radiolabeled RGD Uptake and α_V Integrin Expression Is Enhanced in Ischemic Murine Hindlimbs

Kyung-Han Lee, Kyoung-Ho Jung, Sung-Hee Song, Dong Hyun Kim, Byung Chul Lee, Hyun Ju Sung, Yu-Mi Han, Yearn Seong Choe, Dae Yoon Chi and Byung-Tae Kim

J Nucl Med. 2005;46:472-478.

The Journal of Nuclear Medicine is published monthly.
SNMMI | Society of Nuclear Medicine and Molecular Imaging
1850 Samuel Morse Drive, Reston, VA 20190.
(Print ISSN: 0161-5505, Online ISSN: 2159-662X)

SNMMI SOCIETY OF NUCLEAR MEDICINE AND MOLECULAR IMAGING